

## Charge densities from high-resolution synchrotron X-ray diffraction experiments

Paul R. Mallinson,<sup>a\*</sup> Gordon Barr,<sup>a</sup> Simon J. Coles,<sup>b†</sup> Tayur N. Guru Row,<sup>c</sup> David D. MacNicol,<sup>a</sup> Simon J. Teat<sup>d</sup> and Krzysztof Woźniak<sup>e</sup>

<sup>a</sup>Chemistry Department, University of Glasgow, Glasgow G12 8QQ, UK, <sup>b</sup>Chemistry Department, University of Wales Cardiff, Cardiff CF1 3TB, UK, <sup>c</sup>Solid State and Structural Chemistry Unit and Department of Organic Chemistry, Indian Institute of Science, Bangalore 560 012, India, <sup>d</sup>CLRC Daresbury Laboratory, Daresbury, Warrington WA4 4AD, UK, and <sup>e</sup>Chemistry Department, University of Warsaw, 02-093 Warszawa, ul. Pasteura 1, Poland. E-mail: paul@chem.gla.ac.uk

(Received 27 January 2000; accepted 23 February 2000)

The combination of intense X-ray sources, especially synchrotron radiation, with area-detector technology has accomplished an enormous advance in the experimental conditions available for charge-density analysis by single-crystal high-resolution X-ray diffraction. Such experiments can now be carried out in a time measured in hours rather than weeks. Some features of these experiments are examined and preliminary results are reported for charge-density studies of 2-hydroxy-5-nitrobenzaldehyde *N*-cyclohexylimine (1), octakis(*m*-tolylthio)naphthalene (2), and 7-fluoro-4-styrylcoumarin (3). Weak interactions in crystals of (1) and (3) are found to have similar charge-density characteristics. Cages in the crystal lattice of (2) have a complex charge distribution.

**Keywords:** high-resolution X-ray diffraction; charge density; weak interactions; area detectors; single crystals.

### 1. Introduction

Charge-density (CD) distributions  $\rho(\mathbf{r})$  in molecules and crystals can be determined experimentally using single-crystal high-resolution X-ray diffraction techniques (Coppens, 1997; Spackman, 1998). Bader's theory of 'atoms in molecules' (Bader, 1990), developed on a quantum chemical basis, can be applied to experimentally derived  $\rho(\mathbf{r})$  whence CD properties can be calculated and displayed graphically by means of computer programs such as *XD* (Koritsanszky *et al.*, 1995). Almost in coincidence with these theoretical and computational developments, experimental conditions have improved to the extent that the time required for the X-ray measurements has been reduced from several weeks to one or a few days.

Area detectors are particularly advantageous for CD experiments because of the large data sets required for high-resolution work: reflection data are typically measured up to  $\sin(\theta)/\lambda = 1.1$  or higher. Furthermore, the high-flux X-ray beam from a synchrotron source provides accurate diffraction intensity measurements at such high orders. Since 1995 there have been a number of applications of area detectors [image plate (IP) or charge-coupled device (CCD)], some combined with synchrotron sources,

to experimental CD studies. Table 1 shows an analysis of the various experiments. In some of these, comparisons were made with results from four-circle diffractometer data using a serial (scintillation) detector, and in some cases theoretically derived CD distributions were also obtained.

Bolotovskiy, Darovsky *et al.* (1995) were among the first to demonstrate, in a study of sodium nitroprusside at 100 K, and hexamminechromium(III) hexacyanochromate(III) at 50 K, that synchrotron low-temperature data could be collected with at least the accuracy available with conventional detectors. Graafsma *et al.* (1997) compared two methods of peak integration for the same synchrotron data set, from magnesium formate dihydrate at 100 K. Martin & Pinkerton (1998), using a sealed-tube X-ray source, showed that CCD data for oxalic acid dihydrate at 100 K were adequate for a CD analysis, being at least as good as data from a point detector, and possibly better for weak reflections. In another comparative study, Koritsanszky *et al.* (1998) concluded that the accuracy of a synchrotron/CCD experiment on DL-proline monohydrate, carried out at 100 K in one day, was comparable or even superior to that obtained from a six-week 20 K experiment on DL-aspartic acid with a conventional source and detector. The work of Macchi *et al.* (1998) supports the earlier findings that CCD detectors are well suited for CD studies, by comparing sealed-tube/CCD data for the pharmacological

† Present address: Chemistry Department, University of Southampton, Southampton SO17 1BJ, UK.

**Table 1**  
Charge-density publications involving area detectors.

Diffractometer type	Radiation type (T)			
	Synchrotron radiation (50–100 K)	Mo $K\alpha$ (100–120 K)	Mo $K\alpha$ (20 K)	Ag $K\alpha$ (20 K)
IP (wide frames)	[1] (two compounds)	[9]†		
CCD (wide frames)	[2]‡			
CCD (narrow frames)	[4]§ [12]§ (four compounds) [13] (three compounds)	[3]§ [5]§ [6] [7] [8] [9]† [10] (two polymorphs) [11]§ [12]§		
Four-circle		[3]§ [11]§	[5]§	[4]§ [12]§

† Combined experiment. ‡ Integration via *HIPPO* and *DENZO*. § Comparative experiments. [1] Bolotovskiy, Darovsky *et al.* (1995). [2] Graafsma *et al.* (1997). [3] Martin & Pinkerton (1998). [4] Koritsanszky *et al.* (1998). [5] Macchi *et al.* (1998). [6] Macchi *et al.* (1998a). [7] Macchi *et al.* (1998b). [8] Abramov *et al.* (1998). [9] Scherer *et al.* (1998). [10] Kulkarni *et al.* (1998). [11] Coppens *et al.* (1999). [12] Flaig *et al.* (1999). [13] Mallinson, Wozniak & Guru Row (2000).

compound LR-B/081 at 120 K with point-detector data from the same crystal at 18 K. In a progression from pure technique development, Macchi *et al.* (1998a) report the first complete topological analysis of a C=C double bond coordinated to a transition-metal atom, in bis(5-cyclooctadiene)nickel at 125 K, using the SMART-CCD diffractometer tested in the previous study. The same authors follow this with a study of the metal–metal and metal–ligand bonds in a cobalt complex dimer (Macchi *et al.*, 1998b). Applications to transition-metal compounds were extended with a study of hydrogen bonding in *cis*-HMn(CO)<sub>4</sub>PPh<sub>3</sub> using a SMART-CCD with sealed-tube source at 118 K (Abramov *et al.*, 1998). Another transition-metal study, of a titanium complex, by Scherer *et al.* (1998) employed a novel combination of data at 105 K from a CCD system and from an IP system situated on the same rotating-anode source. Kulkarni *et al.* (1998) compared the CD in two polymorphs of *p*-nitrophenol at 110 K, using a SMART-CCD with sealed-tube source. Coppens *et al.* (1999) studied intermolecular interactions in DL-histidine by CD methods, verifying their 110 K sealed-tube-source SMART-CCD data by comparison with pre-existing CAD-4 diffractometer data.

Comparison of CD results is possible also through studies of chemically equivalent groups in different compounds. In an investigation of possible transferability of electronic properties of molecular and submolecular fragments from amino acids onto larger systems such as oligopeptides, Flaig *et al.* (1999) compared the carboxylate group in four naturally occurring amino acids, using both synchrotron and conventional sources, CCD and point detectors. They found good evidence for the transferability of atomic and group properties. Finally, in the context of comparisons of the topological properties of weak interactions, Mallinson, Wozniak & Guru Row (2000) have obtained synchrotron/CCD data for the three compounds for which preliminary results are reported in this paper.

The foregoing brief survey includes area-detector experiments utilizing conventional and synchrotron X-ray sources. Some considerations arising in one or both of these cases are outlined here.

**Table 2**  
Experimental X-ray data for 2-hydroxy-5-nitrobenzaldehyde *N*-cyclohexylimine (1).

Formula	C <sub>13</sub> H <sub>15</sub> N <sub>2</sub> O <sub>3</sub>
Molecular weight	247.27
Space group (triclinic)	$P\bar{1}$
Temperature (K)	100 (5)
Unit-cell dimensions (Å)	
<i>a</i> (Å)	6.245 (2)
<i>b</i> (Å)	10.097 (3)
<i>c</i> (Å)	10.873 (4)
$\alpha$ (°)	67.23 (3)
$\beta$ (°)	83.46 (2)
$\gamma$ (°)	75.03 (3)
<i>V</i> (Å <sup>3</sup> )	610.6 (4)
<i>Z</i>	2
<i>D<sub>c</sub></i> (g cm <sup>-3</sup> )	1.345
<i>F</i> (000)	262
Crystal dimensions (mm)	0.25 × 0.15 × 0.04
Absorption coefficient (cm <sup>-1</sup> )	0.6
Radiation	SRS, $\lambda = 0.4839$ Å
Frame width	0.2°
( $\sin \theta/\lambda$ ) <sub>max</sub> (Å <sup>-1</sup> )	1.148
( <i>hkl</i> ) lower-limit upper-limit	–14 13; –23 22; –24 24
Beam decay correction	<i>SADABS</i>
Data-collection elapsed time	24 h
No. of reflections measured	32057
No. of symmetry-independent reflections	13603
No. of <i>I</i> > 2σ( <i>I</i> ) reflections	8009
Agreement factor $R = \Sigma I - \bar{I} /\Sigma I$	0.044
Refined on	<i>F</i>
<i>R</i>	0.029
<i>R<sub>w</sub></i>	0.027
<i>S</i>	0.70
<i>N</i> <sub>obs</sub> / <i>N</i> <sub>var</sub>	15.2
Weighting scheme	$w = 1/\sigma^2(F) = 4F^2/\sigma^2(F^2)$
$\sigma^2(F^2) = \sigma_{\text{counting}}^2(F^2) + P^2F^4$ , <i>P</i> = 0.01	

### 1.1. Resolution

(a) For high-resolution work, wavelength is often tuned to approximately 0.48 Å, slightly shorter than the Ag  $K\alpha$  characteristic line. With a detector-to-crystal distance of 4 cm on the Bruker SMART diffractometer, a 100% complete sphere of reciprocal space to 0.45 Å resolution is measured with a single detector setting ( $2\theta = -35^\circ$ ).

**Table 3**Experimental X-ray data for octakis(*m*-tolylthio)naphthalene (2).

Formula	C <sub>66</sub> H <sub>56</sub> S <sub>8</sub>
Molecular weight	1105.68
Space group (tetragonal)	<i>P4/ncc</i>
Temperature (K)	100 (5)
Unit-cell dimensions (Å)	
<i>a</i> (°)	15.749 (1)
<i>c</i> (°)	23.586 (2)
<i>V</i> (Å <sup>3</sup> )	5850.0 (7)
<i>Z</i>	4
<i>D<sub>c</sub></i> (g cm <sup>-3</sup> )	1.255
<i>F</i> (000)	2320
Crystal dimensions (mm)	0.3 × 0.3 × 0.2
Absorption coefficient (cm <sup>-1</sup> )	1.8
Radiation	SRS, λ = 0.4839 Å
Frame width	0.1°
(sin θ/λ) <sub>max</sub> (Å <sup>-1</sup> )	1.155
( <i>hkl</i> ) lower-limit upper-limit	-35 32; -32 36; -54 52
Beam decay correction	<i>SADABS</i>
Data-collection elapsed time	12 h
No. of reflections measured	161925
No. of symmetry-independent reflections	18551
No. of <i>I</i> > 2σ( <i>I</i> ) reflections	7468
Agreement factor <i>R</i> = Σ  <i>I</i> - $\bar{I}$  /Σ <i>I</i>	0.087
Refined on	<i>F</i>
<i>R</i>	0.022
<i>R<sub>w</sub></i>	0.025
<i>S</i>	0.41
<i>N<sub>obs</sub></i> / <i>N<sub>var</sub></i>	14.5
Weighting scheme	$w = 1/\sigma^2(F) = 4F^2/\sigma^2(F^2)$
$\sigma^2(F^2) = \sigma_{\text{counting}}^2(F^2) + P^2F^4$ , <i>P</i> = 0.01	

(b) A short wavelength reduces systematic errors such as absorption and extinction.

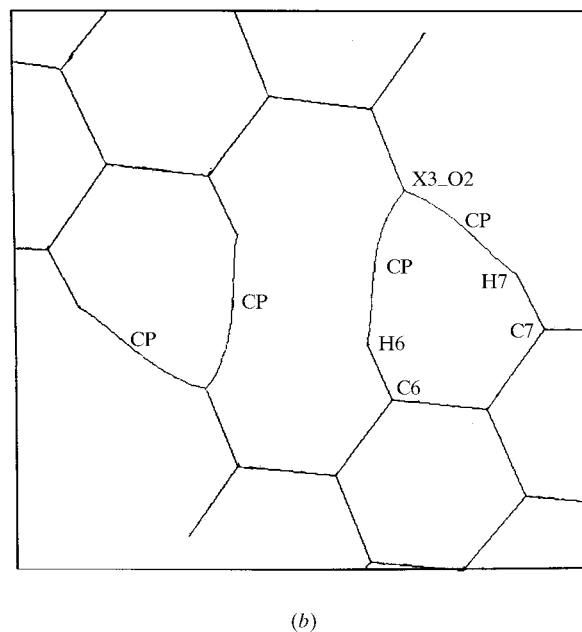
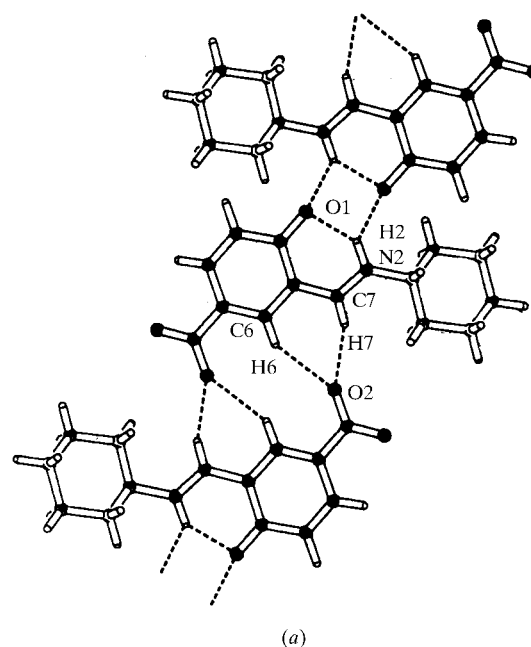
(c) High resolution does not itself affect the total experimental run time when a single detector setting is used. Run time tends to be longer than for normal resolution (structure determination) because (i) a full sphere rather than a hemisphere is measured; (ii) longer exposure is used to measure weak data more accurately, *e.g.* 2 s per frame with synchrotron radiation; (iii) for CCD detectors, narrower frames ( $\omega$  step widths are one-third rather than one-half of the rocking width) are measured so as to improve peak integration. Typical frame width is 0.1°.

### 1.2. Frame width

Using a larger  $\omega$  step width reduces the number of frames required to cover reciprocal space, since more reflections appear on each frame (although there is a possibility of an undesirable overlap of spots). With wide frames ( $\omega$  step width of several degrees) the spots are two-dimensional, but with a step width less than *e.g.* 0.5°, individual spots can extend over several frames and a three-dimensional integration method is employed. An important development in two-dimensional integration, necessarily employed with the wide-frame data obtained from IP detectors, is the 'seed-skewness' method (Bolotovskiy, Darovsky *et al.*, 1995), as embodied in the program *HIPPO* (Bolotovskiy, White *et al.*, 1995).

### 1.3. Detector type

Commercial availability of CCD detectors during the last four years has resulted in them being more widely used than image plates, although the latter are at present cheaper and have a better dynamic range. Overloads characteristic of CCD detectors necessitate re-taking frames with shorter exposure. Although this increases run times, IP detectors have a corresponding disadvantage in

**Figure 1**

(a) A view of part of the crystal structure of (1), showing N-H...O and C-H...O intermolecular interactions as dotted lines. (b) An illustration of C-H...O interaction lines. Symmetry operation: X3\_O2  $-x, -y, -z$ . Symbols CP represent (3, -1) critical points.

**Table 4**  
Experimental X-ray data for 4-styryl-7-fluorocoumarin (3).

Formula	C <sub>17</sub> H <sub>11</sub> FO <sub>2</sub>
Molecular weight	266.27
Space group (monoclinic)	P2 <sub>1</sub> /n
Temperature (K)	100 (5)
Unit-cell dimensions (Å)	
<i>a</i> (Å)	6.782 (2)
<i>b</i> (Å)	20.555 (6)
<i>c</i> (Å)	8.897 (2)
$\beta$ (°)	97.54 (2)
<i>V</i> (Å <sup>3</sup> )	1229.6 (6)
<i>Z</i>	4
<i>D<sub>c</sub></i> (g cm <sup>-3</sup> )	1.438
<i>F</i> (000)	552
Crystal dimensions (mm)	0.6 × 0.2 × 0.2
Absorption coefficient (cm <sup>-1</sup> )	0.6
Range of corrections for absorption by crystal	0.81–1.00
Radiation	SRS, $\lambda = 0.4855$ Å
Frame width	0.1°
( $\sin \theta/\lambda$ ) <sub>max</sub> (Å <sup>-1</sup> )	1.153
( <i>hkl</i> ) lower-limit upper-limit	–15 15; –46 47; –20 20
Beam decay correction	SADABS
Data-collection elapsed time	24 h
No. of reflections measured	83079
No. of symmetry-independent reflections	14788
No. of <i>I</i> > 2 $\sigma$ ( <i>I</i> ) reflections	9247
Agreement factor $R = \Sigma I - \bar{I} /\Sigma I$	0.056
Refined on	<i>F</i>
<i>R</i>	0.032
<i>R<sub>w</sub></i>	0.034
<i>S</i>	0.82
<i>N<sub>obs</sub>/N<sub>var</sub></i>	16.7
Weighting scheme	$w = 1/\sigma^2(F) = 4F^2/\sigma^2(F^2)$
$\sigma^2(F^2) = \sigma_{\text{counting}}^2(F^2) + P^2F^4$ , <i>P</i> = 0.01	
Range of residual density in asymmetric unit (e Å <sup>-3</sup> )	–0.24–0.24

longer readout times. The lack of energy discrimination with both IP and CCD technology introduces the problem of harmonic contamination from the monochromator. This has been shown to be either negligible or easily corrected, both for structure determination and for charge-density experiments (Kirschbaum *et al.*, 1997; Macchi *et al.*, 1998).

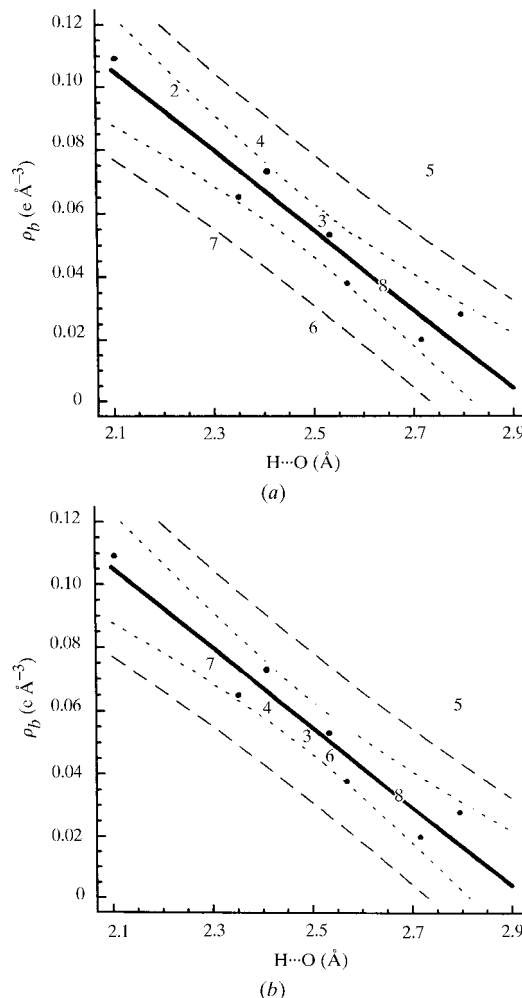
#### 1.4. Beam decay

A feature of synchrotron sources is the periodic decay of incident beam intensity with ring current. This might be allowed for by re-measuring a set of standard frames at intervals, or by utilizing measurements of the incident beam intensity from an ion chamber situated either on the monochromator or on the collimator. Alternatively the correction can be combined with an empirical absorption correction. Blessing's empirical correction (Blessing, 1995) based on intensity measurements for symmetry-equivalent or azimuth-rotation-equivalent reflections depends on there being a substantial multiplicity of these, for at least a low-order subset of the data.

## 2. Experimental

Station 9.8 at the Synchrotron Radiation Source (SRS), CLRC Daresbury Laboratory, is a high-flux single-crystal diffraction facility for use in chemical and materials crystallography (Cernik *et al.*, 1997). It is equipped with a Bruker SMART-CCD detector. The sample crystal is cooled to 100 K with an Oxford Cryostream cooler, to reduce the effects of atomic vibrations on  $\rho(\mathbf{r})$ . A wavelength (0.48–0.49 Å) slightly shorter than the Ag *K* $\alpha$  line enables a resolution of approximately 0.4 Å to be achieved with a single setting of the detector.

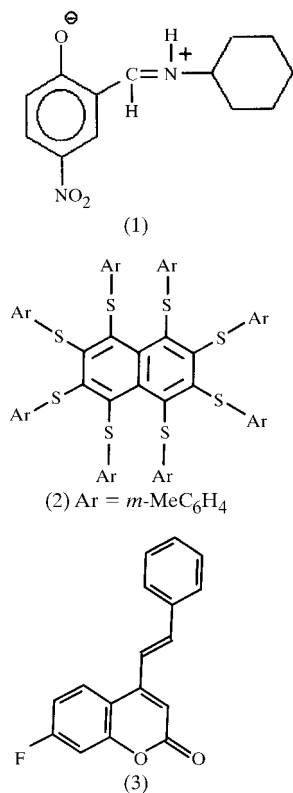
Peak integration and initial data reduction including an empirical absorption correction (Blessing, 1995) were carried out using proprietary software *SAINTE* and *SADABS* (Bruker, 1998), followed by merging of equivalent reflections using *SORTAV* (Blessing, 1989, and references cited therein; Blessing, 1995). Multipole (aspherical atom) refinements and analysis of the CD were carried out using *XD* (Koritsanzky *et al.*, 1995).

**Figure 2**

The relationship between  $\rho_b$  values and H...O acceptor internuclear distances in (1) and (3) (numerals refer to Tables 5 and 6). Dots are data points from Mallinson *et al.* (1997), to which the line is fitted. (a) Experimental  $\rho_b$ ; (b) theoretical  $\rho_b$ .

### 3. Results and discussion

We present here preliminary results from three high-resolution data sets obtained at SRS station 9.8; full reports of the CD analyses are in preparation. The first experiment set out to study intermolecular interactions in compound (1), containing weak hydrogen bonds. Experimental details are given in Table 2. Compound (2) (Table 3) has inclusion host properties in the crystalline state and contains a second-row element, sulfur. Compound (3) (Table 4) is a halogen-containing organic compound in which weak interactions involving halogens are present in the crystal. For (1) and (3), theoretical charge densities were determined by *ab initio* molecular orbital calculations at the Hartree–Fock level of theory, including symmetry-related molecules so as to represent the molecular assembly in the crystals. The calculations were performed with the *GAMESS* package (Schmidt *et al.*, 1993). Topological analysis of these theoretical densities was carried out using the *AIMPAC* suite (Bader, 1985; Biegler-König *et al.*, 1982).



#### 3.1. 2-Hydroxy-5-nitrobenzaldehyde *N*-cyclohexyl imine (1)

This Schiff-base compound has the potential to form both strong and weak intramolecular and intermolecular hydrogen bonds, and in fact both  $N-H \cdots O$  and  $C-H \cdots O$  interactions are found in the crystal (where the molecule exists as a zwitterion), as shown in Table 5 and Fig. 1. For these interactions there is a relationship between the charge density  $\rho_b$  at (3, -1) critical points and donor–

acceptor internuclear distance. Fig. 2 shows this in comparison with data determined earlier for weak interactions in a ‘proton sponge’ compound (Mallinson *et al.*, 1997). Fig. 2 also shows the  $\rho_b$  values for  $C-H \cdots O$  hydrogen bonds in compound (3) (see §3.3). From both the experimental and theoretical results, charge-density characteristics of these weak interactions appear to be consistent in different crystalline compounds.

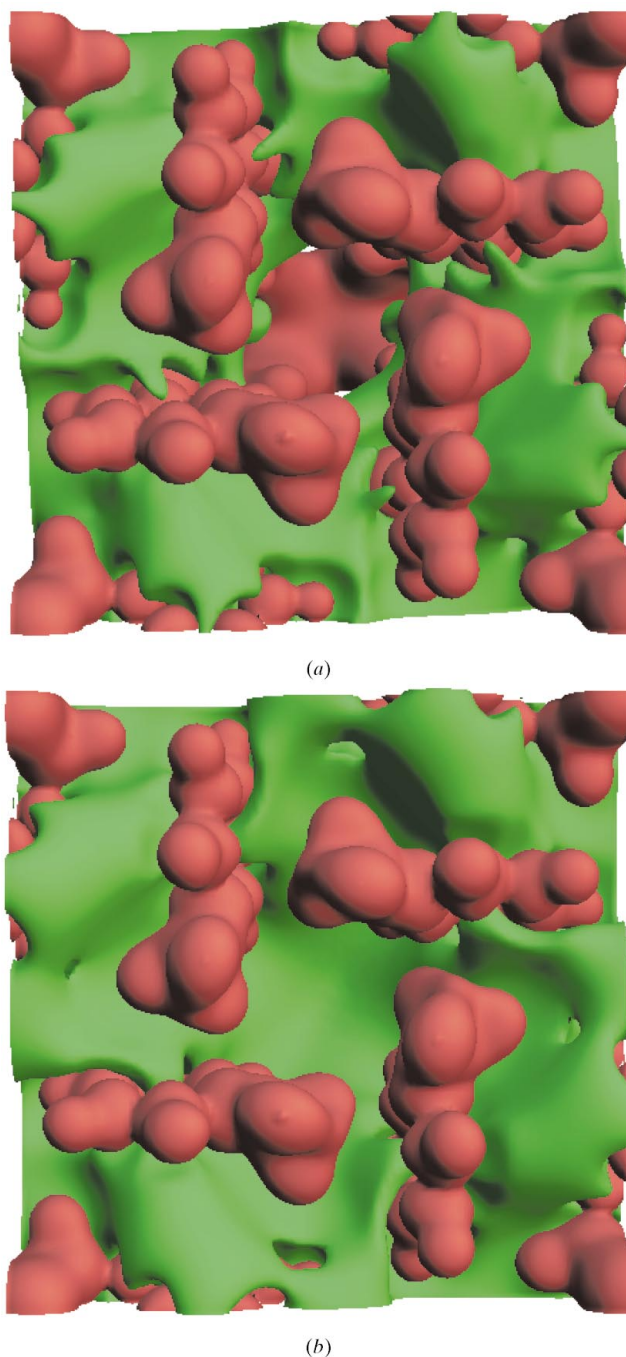


**Figure 3** Electrostatic potential isosurfaces in the crystalline cavity of compound (2). Red surface drawn at  $+0.2 \text{ e } \text{Å}^{-1}$ , green surface at (a)  $-0.3 \text{ e } \text{Å}^{-1}$  and (b)  $-0.2 \text{ e } \text{Å}^{-1}$ .

**Table 5**

Intermolecular interactions in (1)†.

Numbers 1–4 are data points in Fig. 2.

	Internuclear distance (Å)		Angle (°)
1. H2–O1	1.907	N2–H2–O1	136.62
2. H2–X2_O1	2.230	N2–H2–X2_O1	131.90
3. H6–X3_O2	2.515	C6–H6–X3_O2	145.34
4. H7–X3_O2	2.406	C7–H7–X3_O2	149.35

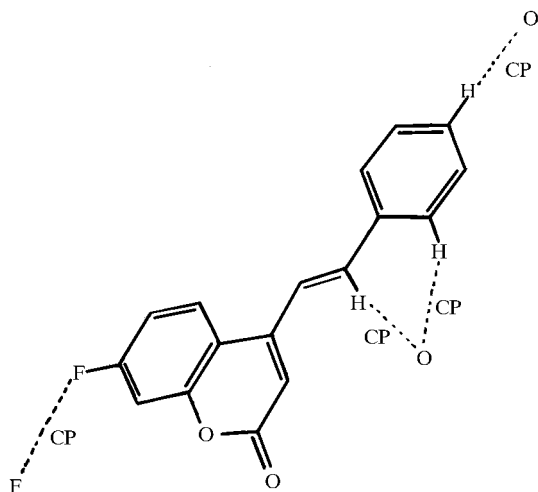
† Symmetry operations: X2\_O1  $1 - x, 1 - y, -z$ ; X3\_O2  $-x, -y, -z$ .

### 3.2. *Octakis(m-tolylthio)naphthalene (2)*

This tetragonal crystal, the structure of which was reported earlier (MacNicol *et al.*, 1985), has the highest symmetry of those studied. The CD in the regions of intermolecular interactions, in the absence of significant hydrogen-bonding effects, is represented by electrostatic potential isosurfaces within the cavity of the crystal structure, shown in Figs. 3(a) and 3(b). The cavity is viewed along the axis of  $\bar{4}$  symmetry. The red isosurface, drawn at  $+0.2 \text{ e } \text{Å}^{-1}$  in both figures, envelopes the nuclei of the atoms forming the cavity walls and floor. The green isosurface is drawn at  $-0.3 \text{ e } \text{Å}^{-1}$  in Fig. 3(a) and  $-0.2 \text{ e } \text{Å}^{-1}$  in Fig. 3(b). The latter surface forms a continuous sheet across the centre of the cavity, while the former contains an opening into the lower half of the cavity, through which the floor can be seen. These features suggest the presence of a region of negative potential, between  $-0.2$  and  $-0.3 \text{ e } \text{Å}^{-1}$  in magnitude, dividing the cavity.

### 3.3. *7-Fluoro-4-styrylcoumarin (3)*

The crystal structure accommodates a short  $\text{F} \cdots \text{F}$  contact as well as weak  $\text{C}-\text{H} \cdots \text{O}$  interactions (Mallinson,

**Figure 4**

An illustration of  $\text{F} \cdots \text{F}$  and  $\text{C}-\text{H} \cdots \text{O}$  interaction lines in crystals of (3). Symbols CP represent (3, -1) critical points.

**Table 6**

Intermolecular interactions in (3)†.

Numbers 5–8 are data points in Fig. 2.

	Internuclear distance (Å)		Angle (°)
5. F1–X3_F1	2.748 (1)	C7–F1–X3_F1	116.08 (3)
6. H16–X2_O2	2.520 (1)	C16–H16–X2_O2	147.84 (3)
7. H12–X3_O2	2.303 (1)	C12–H12–X3_O2	162.94 (3)
8. H14–X3_O2	2.641 (1)	C14–H14–X3_O2	148.95 (3)

† Symmetry operations are: X3\_F1  $-2 - x, -y, 1 - z$ ; X2\_O2  $1/2 - x, 1/2 + y, 1/2 - z$ ; X3\_O2  $-x, -y, -z$ .

Guru Row *et al.*, 2000), shown in Table 6 and Fig. 4. As seen in Fig. 2, the  $\rho_b$  value for the  $\text{F} \cdots \text{F}$  interaction (data point 5) is somewhat removed from the values characteristic of  $\text{C}-\text{H} \cdots \text{O}$  interactions, though of the same order of magnitude. The critical-point properties for the weak hydrogen bonds follow the pattern observed for compound (1).

## 4. Conclusions

More than 20 studies reported over the period 1995–1999 have established revolutionary experimental conditions for the analysis of charge-density distributions in molecules and crystals by high-resolution X-ray diffraction. The combination of synchrotron X-ray source and CCD area detector appears promising for the study of the weaker types of interaction such as  $\text{C}-\text{H} \cdots \text{O}$  and  $\text{F} \cdots \text{F}$ , by topological analysis of the density. A three-dimensional map of the electrostatic potential in the crystalline cavity of an inclusion host compound has also been obtained.

We thank the UK EPSRC for a Visiting Fellowship (GR/M 53981) for TNGR and for beam-time allocation at CLRC (Daresbury, UK). We also thank the Royal Society and the Polish Academy of Sciences for enabling PRM and KW to participate in the European Science Exchange Programme.

## References

- Abramov, Y. A., Brammer, L., Klooster, W. T. & Bullock, R. M. (1998). *Inorg. Chem.* **24**, 6317–6328.
- Bader, R. F. W. (1985). *Acc. Chem. Res.* **18**, 9–15.
- Bader, R. F. W. (1990). *Atoms in Molecules: A Quantum Theory*. Oxford University Press.
- Biegler-König, F. W., Bader, R. F. W. & Tang, T. H. (1982). *J. Comput. Chem.* **3**, 317–328.
- Blessing, R. H. (1989). *J. Appl. Cryst.* **22**, 396–397.
- Blessing, R. H. (1995). *Acta Cryst.* **A51**, 33–38.
- Bolotovskiy, R., Darovsky, A., Kezerashvili, V. & Coppens, P. (1995). *J. Synchrotron Rad.* **2**, 181–184.
- Bolotovskiy, R., White, M. A., Darovsky, A. & Coppens, P. (1995). *J. Appl. Cryst.* **28**, 86–95.

- Bruker (1998). *SAINT, SADABS Area Detector Integration Software*. Madison, Wisconsin, USA.
- Cernik, R. J., Clegg, W., Catlow, R. A., Bushnell-Wye, G., Flaherty, J. V., Greaves, G. N., Burrows, I., Taylor, D. J., Teat, S. J. & Hamichi, M. (1997). *J. Synchrotron Rad.* **4**, 279–286.
- Coppens, P. (1997). *X-ray Charge Densities and Chemical Bonding*. IUCr Texts on Crystallography No. 4. Oxford University Press.
- Coppens, P., Abramov, Y., Carducci, M., Korjov, B., Novozhilova, I., Alhambra, C. & Pressprich, M. R. (1999). *J. Am. Chem. Soc.* **121**, 2585–2593.
- Flaig, R., Koritsanszky, T., Janczak, J., Krane, H.-G., Morgenroth, W. & Luger, P. (1999). *Angew. Chem. Int. Ed.* **38**, 1397–1400.
- Graafsma, H., Svensson, S. O. & Kvik, A. (1997). *J. Appl. Cryst.* **30**, 957–962.
- Kirschbaum, K., Martin, A. & Pinkerton, A. A. (1997). *J. Appl. Cryst.* **30**, 514–516.
- Koritsanszky, T., Flaig, R., Zobel, D., Krane, H.-G., Morgenroth, W. & Luger, P. (1998). *Science*, **279**, 356–358.
- Koritsanszky, T., Howard, S. T., Richter, T., Mallinson, P. R., Su, Z. & Hansen, N. K. (1995). *XD. A Computer Program Package for Multipole Refinement and Analysis of Charge Densities from X-ray Diffraction Data*. Free University of Berlin, Germany; University of Wales, Cardiff, UK; University of Glasgow, UK; University of Buffalo, USA; University of Nancy, France.
- Kulkarni, G. U., Kumaradhas, P. & Rao, C. N. R. (1998). *Chem. Mater.* **10**, 3498–3505.
- Macchi, P., Proserpio, D. M. & Sironi, A. (1998a). *J. Am. Chem. Soc.* **120**, 1447–1455.
- Macchi, P., Proserpio, D. M. & Sironi, A. (1998b). *J. Am. Chem. Soc.* **120**, 13429–13435.
- Macchi, P., Proserpio, D. M., Sironi, A., Soave, R. & Destro, R. (1998). *J. Appl. Cryst.* **31**, 583–588.
- MacNicol, D. D., Mallinson, P. R. & Robertson, C. D. (1985). *Chem. Commun.* pp. 1649–1651.
- Mallinson, P. R., Guru Row, T. N., Prasanna, M. D. & Teat, S. J. (2000). *J. Chem. Soc. Perkin Trans. 2*. Submitted.
- Mallinson, P. R., Wozniak, K., Guru Row, T. N. (2000). In preparation.
- Mallinson, P. R., Wozniak, K., Smith, G. T. & McCormack, K. L. (1997). *J. Am. Chem. Soc.* **119**, 11502–11509.
- Martin, A. & Pinkerton, A. A. (1998). *Acta Cryst.* **B54**, 471–477.
- Scherer, W., Hieringer, W., Spiegler, M., Sirsch, P., McGrady, G. S., Downs, A. J., Haaland, A. & Pedersen, B. (1998). *Chem. Commun.* pp. 2471–2472.
- Schmidt, M. W., Baldrige, K. K., Boatz, J. H., Elbert, S. T., Gordon, M. S., Jensen, J. J., Koseki, S., Matsunaga, N., Nguyen, K. A., Su, S., Windus, T. L., Dupuis, M. & Montgomery, J. A. (1993). *J. Comput. Chem.* **14**, 1347–1363.
- Spackman, M. A. (1998). *Annu. Rep. Prog. Chem. Sect. C*, **94**, 177–207.